



## Impact of particle agglomeration in cyclones

Julio Paiva<sup>a</sup>, Romualdo Salcedo<sup>a,b,\*</sup>, Paulo Araujo<sup>c</sup>

<sup>a</sup> LEPAE, Departamento de Engenharia Química, Faculdade de Engenharia da Universidade do Porto, R. Dr. Roberto Frias, 4200-465 Porto, Portugal

<sup>b</sup> ACS - Advanced Cyclone Systems, SA, Centro de Empresas NET - Edifício PROMONET, Rua de Salzares, 842, 4149-002 Porto, Portugal

<sup>c</sup> CUF - Químicos Industriais, Quinta da Industria, 3860-680 Estarreja, Portugal

### ARTICLE INFO

#### Article history:

Received 24 February 2010

Received in revised form 26 May 2010

Accepted 19 June 2010

#### Keywords:

Optimized cyclones

Turbulent dispersion

Particle agglomeration

### ABSTRACT

The purpose of this work is to build a model to predict in a more realistic way the collection efficiency of gas cyclones, and in particular, of numerically optimized cyclones, that show very high collection efficiencies for sub-micrometer particles. These cyclones can be coupled to recirculation systems for further improving the collection efficiencies of these fine particles.

As a first approach, in this paper a reverse-flow gas-cyclone without recirculation was studied. The model starts by solving the particle trajectory in a predetermined flow field inside the cyclone on which turbulence is superimposed by adding random fluctuating components. By employing a fixed set of parameters, it determines if a collision or an agglomeration occurs. In case of agglomeration, the initial particles will have a dynamic behavior inside the cyclone as a newly formed agglomerate, thus having a different collection efficiency from that of the original particles. In fact, the observed efficiency will increase above theoretical predictions for un-agglomerated particles and this can be observed in various experimental results.

The hypothesis of particle agglomeration within the cyclone turbulent flow seems a sound justification for the higher than predicted collection efficiencies observed for smaller particles in a gas-cyclone, being expectable with recirculation that this effect will become even more significant.

© 2010 Elsevier B.V. All rights reserved.

### 1. Introduction

Collection efficiency models currently developed for gas cyclones, such as the Mothes and Löffler's model [1], can predict with good accuracy the collection efficiency of particles with diameters above about 2–3  $\mu\text{m}$ .

Experimentally, several authors have observed at laboratory, pilot and industrial-scales [2–10] that cyclone systems can have much higher collection for fine particles (below about 3  $\mu\text{m}$ ) than predicted by classical models, viz. grade-efficiency curves may show a minimum in collection at an intermediate particle size (ranging from about 0.8 to 2  $\mu\text{m}$ ). Since these hook-like curves do not always occur [2,7], the phenomenon, whatever its cause, is probably dependent on the physical properties of the powders, on the gas flow field inside the cyclone or on both.

Muschelknautz's model [7,11–13] predicts, at high solid loadings, a fairly constant value of collection efficiency for the smaller

particles, since it is postulated that a portion of the feed is separated unclassified, but it does not predict the abnormal high collection for fine particles observed for dilute systems at low or moderate loadings (feed concentrations 1–10  $\text{g}_{\text{powder}}/\text{m}_{\text{gas}}^3$ ).

This work proposes that this abnormal behavior for fine particles is attributed to agglomeration within the cyclone turbulent flow field, as initially postulated by Mothes and Löffler [14], much as it happens in recirculating fluidized beds [15,16]. This phenomenon is modeled by considering the particles' trajectories inside the cyclone and the probability of interparticle collisions. If some of these collisions result in effective particle agglomeration, one of the direct implications is that the particle size distribution actually processed by the gas cyclone differs from the feed size distribution, increasing the overall collection efficiency for these systems.

Upon agglomeration of fine particles by larger ones, the smaller particles will be captured as much larger particles, viz. with much higher collection efficiency than that predicted by any of the currently available models. If the cyclone is highly efficient above about 2–3  $\mu\text{m}$ , i.e., above 90–95% collection, as it indeed happens with high efficiency cyclone systems, and especially with recirculation systems and numerically optimized cyclones [2,9], then the smaller particles will also be collected with these high efficiencies, and this could explain the minima observed in many grade-efficiency curves. As a direct consequence, the more efficient the cyclone

Abbreviations: PACyc, particle agglomeration in cyclones; PSD, particle size distribution.

\* Corresponding author at: LEPAE, Departamento de Engenharia Química, Faculdade de Engenharia da Universidade do Porto, R. Dr. Roberto Frias, 4200-465 Porto, Portugal.

E-mail address: [rsalcedo@fe.up.pt](mailto:rsalcedo@fe.up.pt) (R. Salcedo).

## Nomenclature

$a$	gas entry height (m)
$A$	Hamaker constant (J)
$b$	gas entry width (m)
$C$	mass concentration ( $\text{kg m}^{-3}$ )
$c_D$	drag coefficient
$c_T$	Lagrange constant
$D$	cyclone diameter (m)
$D_{new}$	new agglomerate diameter (m)
$d_p$	particle diameter (m)
$d_{p,i}$	diameter of particle $i$ (m)
$d_{trun}$	cut-off diameter class
$D_A$	diameter of particle $A$ (m)
$D_B$	diameter of particle $B$ (m)
$D_b$	particle exit diameter (m)
$D_C$	diameter of particle $C$ (m)
$D_e$	gas exit diameter (m)
$D_{final,i}$	is the last of the final diameters that belongs to class $i$
$D_{initial,i}$	is the first of the final diameters that belongs to class $i$
$D_r$	radial turbulent dispersion
$e$	energetic restitution coefficient
$f$	friction factor
$f(\Delta r)_i$	longitudinal correlation coefficient in direction $i$
$f_c$	collision frequency combining turbulent inertia and differential settling
$f_c^{Brown}$	collision frequency only by Brownian diffusion
$f_{n,i}$	fraction of class $i$ in non-cumulative number distribution
$f_{w,i}$	fraction of class $i$ in non-cumulative mass distribution
$g_i$	acceleration in direction $i$ ( $\text{m s}^{-2}$ )
$g(\Delta r)_i$	transverse correlation coefficient in direction $i$
$H$	cyclone height (m)
$H_c$	cyclone cylinder diameter (m)
$h_z$	equivalent height of cylinder gas cyclone (m)
INFO	structure with all identification of $i$ particles that shifted to $j$ class
$k$	turbulent kinetic energy ( $\text{m}^2 \text{s}^{-2}$ )
$k_B$	Boltzmann constant ( $\text{J K}^{-1}$ )
$K$	angular momentum parameter
$m_{total}$	total mass particle inside the gas cyclone (kg)
$N_c$	total number of collisions
$N_{classes}$	total number of classes
$N_{final}$	last of the final number of diameters belonging to a class
$n_{i,j}$	number of particles initially belonging to class $i$ that shifted to class $j$
$n_{injected,i}$	number of particles of class $i$ injected in control volume
$N_{initial}$	first of the final number of diameters belonging to a class
$n_{original,i}$	number of particles in proportion in class $i$
$n_{p,i}$	number of particles in class $i$
$n_{real,i}$	actual number of particles in class $i$
$N_{slices}$	number of slices
$N(0, 1)$	random number (standard normal distribution)
$P_{collision}$	collision probability
$p_{pl}$	material limiting contact (Pa)
$Pe_p$	radial particle Peclet number
$r$	radial coordinate (m)
$r_w$	external radius of the cyclone (m)

$R_{E,i}(\Delta r)$	Eulerian part of turbulent correlation function
$R_{p,i}(\Delta t, \Delta r)$	turbulent correlation function in direction $i$
$R_L(\Delta t)$	Lagrangian part of turbulent correlation function
$Re_p$	particle Reynolds number
$Re_p^R$	radial particle Reynolds number
$ss$	distance of the gas exit to the top of the cyclone (m)
$t$	instant of time (s)
$T_L$	Lagrangian integral time scale (s)
$u_d$	downward gas velocity inside the cyclone ( $\text{m s}^{-1}$ )
$u_{fluid,i}$	fluid velocity component in direction $i$ ( $\text{m s}^{-1}$ )
$u_{fluid,i}^n$	fluid velocity component in direction $i$ in time step $n$ ( $\text{m s}^{-1}$ )
$u_{fluid,i}^{n+1}$	fluid velocity component in direction $i$ in time step $n+1$ ( $\text{m s}^{-1}$ )
$u_{fluid}^r$	radial fluid velocity proposed by Mothes and Löffler ( $\text{m s}^{-1}$ )
$u_{fluid}^t$	tangential fluid velocity proposed by Mothes and Löffler ( $\text{m s}^{-1}$ )
$u_{fluid}^{t,*}$	tangential fluid velocity after vena contracta effect ( $\text{m s}^{-1}$ )
$u_{p,i}^N$	velocity component in $i$ direction of particle $N$ ( $\text{m s}^{-1}$ )
$u_r$	radial fluid velocity ( $\text{m s}^{-1}$ )
$U(0, 1)$	random number (uniform distribution)
$v_{cr}$	critical velocity ( $\text{m s}^{-1}$ )
$V_{control}$	control volume's volume ( $\text{m}^3$ )
$V_{cyclone}$	cyclone volume ( $\text{m}^3$ )
$V_{fluid}$	total fluid's volume in the control volume ( $\text{m}^3$ )
$V_{particles}$	total particle's volume in the control volume ( $\text{m}^3$ )
$V_{particles,injected}$	volume of the injected particles ( $\text{m}^3$ )
$x_{p,i}^N$	position of particle $N$ in $i$ direction (m)
$Z_0$	contact distance (m)
$\alpha$	ratio between fluid and particle volumes
$\beta$	entry parameter
$\Delta r$	displacement (m)
$\Delta t$	time step (s)
$\epsilon$	cyclone cone angle (rad)
$\eta_i^{final}$	collection efficiency of particles belonging to class $i$ proposed by Mothes and Löffler
$\eta_i^{final,*}$	final collection efficiency after agglomeration of a particle belonging to class $i$
$\eta_i^{slice}$	collection efficiency of particles belonging to class $i$ in each slice
$\eta_j^{slice,*}$	final collection efficiency after agglomeration of a particle belonging to class $j$ per slice
$\mu$	fluid viscosity ( $\text{kg m}^{-1} \text{s}^{-1}$ )
$\phi$	collision angle (rad)
$\rho$	specific gravity of the fluid ( $\text{kg m}^{-3}$ )
$\sigma_F$	mean fluctuation of fluid velocity at the particle position ( $\text{m s}^{-1}$ )
$\tau$	mean residence time (s)
$\varepsilon$	dissipation velocity of turbulent kinetic energy ( $\text{m}^2 \text{s}^{-3}$ )
$\vec{u}_{fluid}$	fluid velocity ( $\text{m s}^{-1}$ )
$\vec{u}_{new}$	new agglomerate velocity ( $\text{m s}^{-1}$ )
$\vec{u}_p^N$	velocity of particle $N$ ( $\text{m s}^{-1}$ )
$\vec{u}_{p1}$	particle 1 velocity after collision with no agglomeration ( $\text{m s}^{-1}$ )
$\vec{u}_{p2}$	particle 2 velocity after collision with no agglomeration ( $\text{m s}^{-1}$ )

for (unagglomerated) particles above about 2–3 μm, the more pronounced will the hook-like grade-efficiency curves become.

**2. PACyc model—particle agglomeration in cyclones**

The PACyc model (Particle Agglomeration in Cyclones) was developed to predict the phenomenon of particle collection in reverse flow cyclones by taking into account the agglomeration phenomenon in turbulent flows.

*2.1. Introducing the PACyc model*

The purpose of the PACyc model is to predict cyclone collection efficiency, both grade and global, in reverse-flow cyclone collectors, as stand-alone units or within recirculation systems [2], and, in particular, for a cyclone geometry that was obtained through numerical optimization [17].

In the PACyc model, for purposes of interpretation, there are two types of particles: target and colliders. Only binary (two-body particle-to-particle) interactions are allowed, and all diameters are considered as target particles, provided collider particles are not larger than the target particles.

In terms of its main constituents, the PACyc model adopts the Mothes and Löffler model [1] as a good estimate for the collection efficiency of particles of any diameter. This model is used to build a baseline for the grade-efficiency curves, i.e., without agglomeration. The Mothes and Löffler model has as unknown parameter the particles' turbulent dispersion coefficient, which is here calculated according to Salcedo and Coelho [5]. For this, an analogy is made between turbulent dispersion of the solid phase in cyclone flow and turbulent dispersion processes in flows through packed beds. The empirical expression used to calculate the turbulent dispersion coefficient is shown in Eq. (1),

$$Pe_p = 0.0342 (Re_p^R)^{1.263} \tag{1}$$

where  $Pe_p = u_r d_p / D_r$  is the radial Peclet number,  $D_r$  is the radial dispersion coefficient and  $Re_p^R = \rho d_p u_r / \mu$  is the radial particle Reynolds number.

After building the baseline curves, PACyc couples the model proposed by Sommerfeld [15,18] to obtain the modified (final) grade-efficiency curves. These steps are explained below.

*2.2. Reverse-flow cyclone efficiency estimation*

There are several models available to predict the collection efficiency in reverse-flow gas-cyclones. Previous work [3,19,20] has shown that the Mothes and Löffler model [1] gives, on average, the best agreement with available data. Thus, this model was retained as the model used to predict grade-efficiency in cyclones, in the absence of particle collision/agglomeration.

The main hypothesis assumed in the Mothes and Löffler model are:

- The cyclone flow-field is divided in 4 parts: the entrance area, the downstream flow region, the re-entrainment region and the region of upstream flow;
- The tangential velocity depends only on the radial coordinate and not on the axial coordinate;
- The particle motion is determined as the sum of a random movement (due to the gas turbulence) and a deterministic movement (due to the flow of particles in the centrifugal field);
- For the removal of particles from the gas, particles entering the upward inner vortex are lost. Particles colliding with the cyclone wall are captured;
- Reentrainment of already deposited particles from the conical part is essentially due to the increasing turbulent back mixing of

**Table 1**  
Ratio between Sommerfeld and Brownian collision rates for the smaller diameters.

$\frac{f_c}{f_c^{Brown}}$	Collider diameter (μm)							
	0.135	0.265	0.350	0.450	0.575	0.725	0.900	...
Target diameter (μm)								
0.135	9	0	0	0	0	0	0	...
0.265	20	43	0	0	0	0	0	...
0.350	35	67	90	0	0	0	0	...
0.450	36	76	109	143	0	0	0	...
0.575	51	115	149	199	247	0	0	...
0.725	44	152	221	276	359	434	0	...
0.900	156	207	337	422	542	651	755	...
...	...	...	...	...	...	...	...	...

particles near the cyclone bottom. Reentrainment was however ignored in the present paper.

In order to determine the collection efficiency, a mass balance is established between the region of escaping particles (upstream flow) and the entry area.

*2.3. Interparticle agglomeration*

The agglomeration effect taken into account in PACyc is based on the Sommerfeld model [15,18] of particle agglomeration in turbulent flows.

In purely viscous or transitional flow, submicrometric particle agglomeration is mainly due to Brownian diffusion [21] and an expression to determine the collision rate by this mechanism is given in Eq. (2), proposed by Smoluchowski (as quoted by Elimelech [22]),

$$f_c^{Brown} = \frac{2 k_B T (d_{p,1} + d_{p,2})^2}{3 \mu d_{p,1} d_{p,2}} \tag{2}$$

where  $k_B$  is Boltzmann's constant,  $T$  is the absolute temperature,  $\mu$  is the fluid dynamic viscosity and  $d_{p,1}$  and  $d_{p,2}$  are the particles diameters for a binary interaction.

However, in turbulent flows such as those occurring in gas cyclones, this is not so. Sommerfeld [15] proposes that in a Eulerian/Lagrangian referential as all particles are larger than the turbulent length scales involved in the agglomeration process, turbulent inertia and differential settling (shear) are the relevant mechanisms for particle collision. The collision frequency ( $f_c$ ) of one particle (i.e.  $n_{p,i} = 1$ ) with diameter  $d_{p,i}$  and velocity  $\vec{u}_{p,i}$  with all other particles with diameter  $d_{p,j}$  and velocity  $\vec{u}_{p,j}$  can be calculated according to the kinetic theory of gases using Eq. (3).

$$f_c = \frac{N_c}{n_{p,i}} = \sum_{j=1}^{N_{class}} \frac{\pi}{4} (d_{p,1} + d_{p,2})^2 \left| \vec{u}_{p,1} - \vec{u}_{p,2} \right| n_{p,j} \tag{3}$$

The main assumptions (proposed by Sommerfeld [15,18]) associated with the use of Eq. (3) are the following:

- The particle number concentration is small enough that the occurrence of binary collisions prevail;
- On the other hand the particle concentration must be large enough to allow a statistical treatment;
- The velocities of the colliding particles are not directly correlated.

To verify which collision mechanism is dominant, Table 1 shows a sample of the ratio between Sommerfeld's collision frequency [15] (Eq. (3)) and Brownian diffusion collision frequency (Eq. (2)).

Considering the ratios presented in Table 1, it is possible to conclude that the results of the combined mechanisms proposed by Sommerfeld [15] is clearly dominant over that for Brownian diffusion.

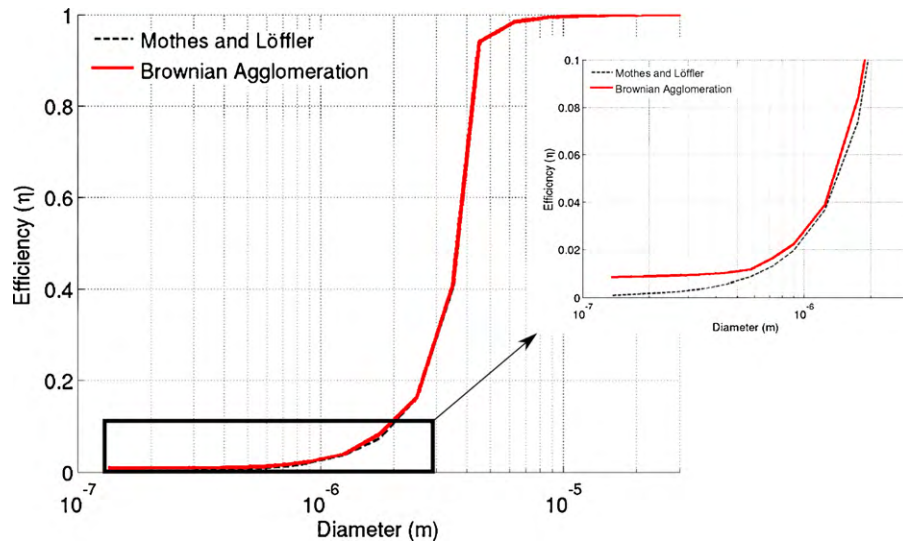


Fig. 1. Grade-efficiency for Brownian induced agglomeration.

In order to test the hypothesis of Brownian agglomeration being responsible for the higher than predicted collection efficiency of the smaller particles, a simulation was made (in the conditions of our experiments), considering Brownian diffusion as the only agglomeration mechanism. Fig. 1 shows the results of this simulation and it is possible to conclude that for our hypothesis, Brownian agglomeration is a phenomenon that does not explain, by itself, the observed behavior of the finest particles.

Also, previous simulation work in fluidized-beds [16], with particle number concentration similar to the ones in our systems, has shown that change in the fine particle number density distribution due to agglomeration by Brownian motion can be neglected when compared to the corresponding change due to turbulence/shear (even for particles as small as  $0.2\ \mu\text{m}$  in diameter). Recently, Lipowsky and Sommerfeld [23] and Sommerfeld and Lain [24] also neglect Brownian agglomeration when predicting cyclone collection with interparticle agglomeration.

Another evidence to support neglecting Brownian diffusion can be found in Elimelech [22], since for agglomeration by this mechanism to be relevant in reducing the particle number concentration, a very appreciable time (of the order of the 1000 time constants) is needed. In our case, for a  $25\ \mu\text{m}$  target particle and for an  $0.135\ \mu\text{m}$  injected particle, this translates in  $\approx 20\text{ s}$  and this is the best scenario for Brownian agglomeration. For  $0.135\ \mu\text{m}$  target particles, this time would increase to  $\approx 900\text{ s}$ . Considering the fact that in the studied system, the maximum contact times of the particles inside the gas cyclone is less than 1s, Brownian agglomeration has insufficient time to be relevant, and was thus ignored in the present work.

Fig. 2 is a representative outline of the proposed agglomeration algorithm.

One of the initial steps of this analysis is that the model should evaluate a control volume equal (in size and shape) to the cyclone under study. Considering that the Mothes and Löffler [1] model proposes as a simplification a volume-equivalent cylindrical gas-cyclone, the control volume used in PACyc has the same volume but not the same geometry as the real gas-cyclone.

The model starts by assuming particles that enter the cyclone to be uniformly distributed in the annular space between the cyclone inner wall and the vortex finder outer wall. Since the Mothes and Löffler model proposes that collection efficiency is independent of the axial coordinate, it was assumed that the 3D control volume can be represented by a 2D control surface.

The data used by PACyc is arranged in 4 groups: geometric data (geometry of the system), operation data (operating conditions, such as pressure, temperature, gas flow rate, . . .), particle information (characteristics of particles such as mass distribution, specific gravity, . . .) and interaction data (interaction step, interaction end-time, . . .). Each of these groups has a different impact on the final result, but the geometric and operation data are mainly used to predict the initial efficiency, while part of the particles' data and the interaction data are used for the agglomeration impact on the final collection efficiency.

The model starts by calculating the fluid velocity in the control volume, and then studies the trajectories of each individual particle injected in this control volume.

Following the Sommerfeld model, Eq. (4) solves the particle trajectory explicitly while Eq. (5) calculates the particle velocity. In this work, the DDASPK solver [25] was used to integrate these equations. These calculations are directly related to some physical parameters such as the fluid and particle specific gravities and the relative velocity between the particle and the fluid. The drag coefficient ( $C_D$ ) is obtained using a standard correlation given in

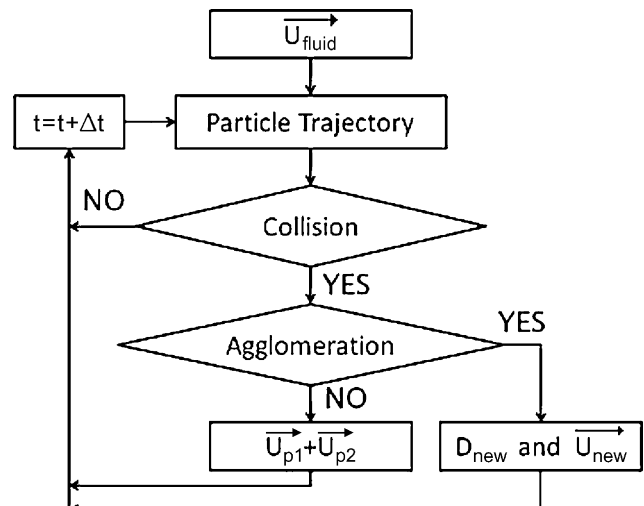


Fig. 2. Representation of the interparticle agglomeration model.

Eq. (6), and the particle's Reynolds number ( $Re_p$ ) is given by Eq. (7).

$$\frac{dx_{p,i}^N}{dt} = u_{p,i}^N \quad N = 1 \dots N_{particles} \quad (4)$$

$$\frac{du_{p,i}^N}{dt} = \frac{3}{4} \frac{\rho c_D}{\rho_p d_p^N} (u_{fluid,i} - u_{p,i}^N) \left\| \vec{u}_{fluid} - \vec{u}_p^N \right\| + g_i \quad N = 1 \dots N_{particles} \quad (5)$$

$$c_D = \begin{cases} \frac{24}{Re_p} (1.0 + 0.15 Re_p^{0.687}), & Re_p < 1000 \\ 0.44, & Re_p \geq 1000 \end{cases} \quad (6)$$

$$Re_p = \frac{\rho \left\| \vec{u}_{fluid} - \vec{u}_p \right\| d_p}{\mu} \quad (7)$$

In this work we only consider that the gas phase influences the solid phase, viz. a one-way coupling. Meier and Mori [26] have shown, for a solids' volume fraction of  $3.38 \times 10^{-6}$ , that two-way coupling reduces the tangential velocities, but even near the cyclone wall, where the solids volume fraction is larger (between  $2.0 \times 10^{-3}$  and  $10^{-2}$ ), the difference is quite small (about  $0.3 \text{ m s}^{-1}$  reduction in the tangential velocity). Considering that for all cases reported in this manuscript (including the experimental cases) the volume fraction of solids is between  $2.0 \times 10^{-6}$  and  $6.7 \times 10^{-6}$ , it is plausible to consider all our systems as dilute, justifying the one-way coupling strategy.

Solving Eqs. (4)–(7) in a predetermined flow field leads each particle to have a deterministic behavior in the control volume. However, for the PACyc model, turbulent random fluctuations are superimposed to this predetermined flow field. Obviously, using a different predetermined gas flow field will yield different grade-efficiency curves, due to the different baseline grade-efficiencies. Mothes and Löffler [1] estimate the radial dependence of the tangential velocity by the cyclone geometry and wall roughness through Eq. (8),

$$u_{fluid}^r = \frac{u_{fluid}^t}{(r)/(r_w)[1 + K(1 - (r)/(r_w))]} \quad (8)$$

where the tangential velocity at the external radius of the cyclone body is given by Eq. (9).

$$u_{fluid}^t = \frac{u_d}{f h_z} \left[ \left( 0.25 + \frac{f h_z u_w}{u_d} \right)^{0.5} - 0.5 \right] \quad (9)$$

For Eqs. (8) and (9), the relations (10)–(14) are applied.

$$u_d = \frac{Q}{\pi r_w^2} \quad (10)$$

$$u_w^* = \frac{Q}{\pi a b \beta} \quad (11)$$

$$\beta = -0.204 \frac{b}{r_w} + 0.889 \quad (12)$$

$$h_z = \frac{a}{h_z} \left[ \frac{2\pi - \arccos[(b)/(r_w) - 1]}{2\pi - 1} \right] + \frac{h}{r_w} \quad (13)$$

$$K \approx \frac{u_{fluid}^t}{u_d} \left[ 1 + \frac{f}{\sin \epsilon} \right] \quad (14)$$

Additionally, the variation of the tangential velocity with the axial coordinate is not considered, as this dependence is very weak [1,27].

To introduce turbulence into the system, using the Sommerfeld model [15,18], the fluid velocity is updated, in consecutive time

steps and at each position, according to Eq. (15),

$$u_{fluid,i}^{n+1} = u_{fluid,i}^n R_{p,i}(\Delta t, \Delta r) + \left| u_{fluid,i}^n \right| \sqrt{1 - [R_{p,i}(\Delta t, \Delta r)]^2} \times N(0, 1) \quad (15)$$

where  $N(0, 1)$  is a random number generated from a standard normal distribution. The first term on the right-side represents the correlated part and the second term the random contribution to the velocity fluctuation. The correlation function ( $R_{p,i}(\Delta t, \Delta r)$ ) is composed of a Lagrangian and an Eulerian part, in order to account for the crossing trajectories in the case when gravity is considered, and is shown in Eq. (16),

$$R_{p,i}(\Delta t, \Delta r) = R_L(\Delta t) \times R_{E,i}(\Delta r) \quad (16)$$

where the index  $i$  stands for each of the component  $x$  and  $y$  directions. For the Lagrangian auto-correlation function, an exponential form is selected, as shown in Eq. (17).

$$R_L(\Delta t) = \exp\left(-\frac{\Delta t}{T_L}\right) \quad (17)$$

In this equation the Lagrangian integral time scale ( $T_L$ ) is determined from Eq. (18), and the mean fluctuation of the fluid at the particle's position ( $\sigma_F$ ) is given by Eq. (19), as defined from kinetic theory.

$$T_L = c_T \frac{\sigma_F^2}{\epsilon}, \quad c_T = 0.4 \quad (18)$$

$$\sigma_F = \frac{2k}{3} \quad (19)$$

The spacial correlation of the individual velocity components for two arbitrary points in space can be obtained by the Eulerian correlation tensor ( $R_{e,ij}(\Delta r)$ ) (using Eq. (20)), by using the longitudinal ( $f(\Delta r)$ ) and transverse ( $g(\Delta r)$ ) correlation coefficients, given by Eqs. (21) and (22).

$$R_{e,ij}(\Delta r) = [f(\Delta r)_i - g(\Delta r)_i] \frac{r_i r_j}{r^2} + g(\Delta r)_i \delta_{ij} \quad (20)$$

$$f(\Delta r)_i = \exp\left(-\frac{\Delta r}{L_{E,i}}\right) \quad (21)$$

$$g(\Delta r)_i = \left(1 - \frac{\Delta r}{2L_{E,i}}\right) \exp\left(-\frac{\Delta r}{L_{E,i}}\right) \quad (22)$$

The integral length scales for each direction were determined by Eq. (23), considering stream-wise component as  $x$  and transverse component as  $y$ .

$$L_{E,x} = 1.1 T_L \sigma_F, \quad L_{E,y} = 0.5 L_{E,x} \quad (23)$$

All the parameters associated with turbulence are taken into account in the value of the turbulent correlation function  $R_{p,i}(\Delta t, \Delta r)$  which is bounded to  $[0, 1]$ . As a short explanation of the impact of this variable in the final fluid velocity field, if  $R_{p,i}(\Delta t, \Delta r)$  has a value near one, the velocity of the fluid is highly correlated in consecutive time steps, so turbulence is low and the fluid velocity has almost a deterministic behavior. However, if  $R_{p,i}(\Delta t, \Delta r)$  has a value near zero, the velocity autocorrelation function decays quickly to zero, implying a strong turbulent flow and consequent almost random behavior of the fluid velocity between consecutive time steps.

After obtaining the particles' trajectories in turbulent flow, a statistical criteria (collision probability) is used to determine if a collision occurs between two particles.

The probability of collision is essentially the number of collisions within a time step, and is calculated as the product of the time step

$\Delta t$  and the collision frequency, as given by Eq. (24),

$$P_{collision} = \frac{\pi}{4} (d_{p,1} + d_{p,2})^2 \left\| \vec{u}_{p,1} - \vec{u}_{p,2} \right\| N_p \Delta t \quad (24)$$

where  $d_{p,1}$  and  $d_{p,2}$  correspond to the particles' diameters,  $\left\| \vec{u}_{p,1} - \vec{u}_{p,2} \right\|$  is the euclidean norm of the relative velocity and  $N_p$  is the total number concentration.

The model compares the collision probability with a random number  $U(0, 1)$  generated from a uniform distribution, and considers that a collision occurs when  $U(0, 1) < P_{collision}$ .

In the absence of collision, each particle is reinjected in the next time step with its velocity unmodified.

In the case of collision, an energy criterion is used to decide whether the result of the collision is an agglomerate. Considering only Van der Waals forces, the critical velocity ( $v_{cr}$ ) is determined by Eq. (25),

$$v_{cr} = \frac{1}{d_{p,2}} \frac{\sqrt{1-e^2}}{e^2} \frac{A}{\pi z_0^2 \sqrt{6} p_{pl} \rho_p} \quad (25)$$

where  $e$  is the energy restitution coefficient,  $A$  is the Hamaker constant,  $z_0$  is the contact distance and  $p_{pl}$  is the material limiting contact pressure, all of these assigned by default with the values proposed by Sommerfeld [15,18].

The model proposes that an agglomerate is formed when the normal relative velocity ( $\left\| \vec{u}_{p,1} - \vec{u}_{p,2} \right\| \cos \phi$ ) is not larger than the critical velocity.

Otherwise, the model considers momentum conservation and calculates the new velocities of the two resulting particles after interaction.

If agglomeration occurs, the model calculates the size of the new cluster and its velocity, taking into account not only momentum but also mass conservation. As a simplification, a spherical agglomerate (with the mass of both particles) is considered as the outcome of the agglomeration process.

All the particles are injected in a combinatorial way, where the binary interactions are randomly analyzed in each time step, updating the fluid velocity and the particles' positions. Typically, each binary interaction takes about 10 ms per 100 particles, 300 ms per 1000 particles, 30 s per 10k particles and 400 s per 100k particles in an AMD 3.0 GHz Dual-Core Athlon 64bits processor. This process is repeated until the final time of interaction, defined by the combination of geometrical and operation data, is reached.

### 2.3.1. Control volume definition

The cyclone standard configuration is presented in Fig. 3.

The control volume taken into account corresponds to the region occupied by the outer vortex, as given by the gray region of Fig. 4. The main impact of neglecting the inner core is on the reduction of the contact time of the particles.

It is assumed that particles that eventually end-up in the inner vortex, become unavailable for collisions, and thus, are not relevant in promoting agglomeration and in increasing the collection efficiency for the smaller particles. Thus, these particles are not reinjected in the cyclone in the next time step. The collisions that would eventually occur in the inner vortex are neglected, by considering their collision probability equal to zero.

The particles that reach the outer wall of the cyclone are also considered unavailable for collisions being also assigned a null collision probability. Thus, particle rebound at the cyclone walls is not allowed.

To circumvent the simplification of the separation in the cyclone being independent of the axial coordinate, the gas-cyclone can be divided in a user-defined number of slices. Each slice is assigned a base collection efficiency, i.e., without agglomeration, in such a way that the overall efficiency summed over all slices corresponds

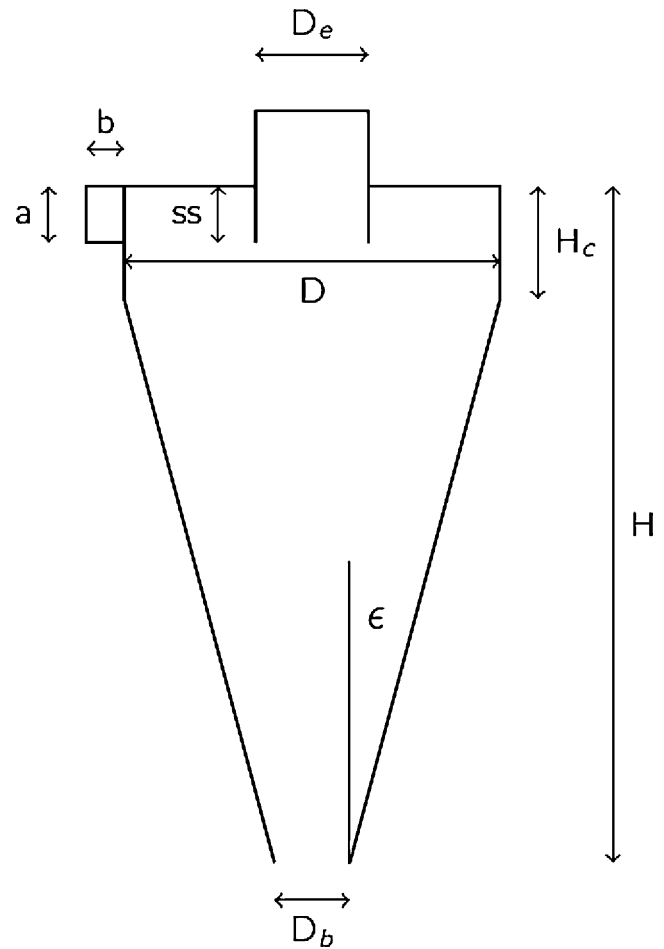


Fig. 3. Geometrical variable identification in cyclone.

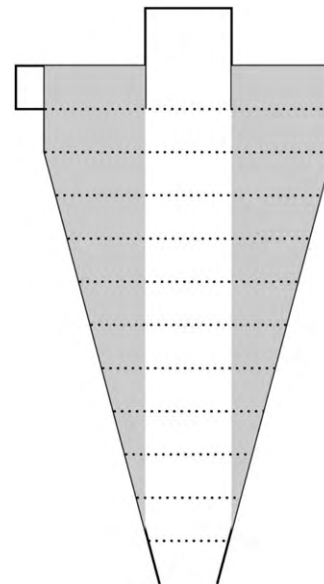


Fig. 4. Setting the volume control (outer vortex and slices).

to the overall collection efficiency proposed by Mothes and Löffler [1].

Hence, the final control volume is as shown in Fig. 4, and the slice collection efficiency is given by Eq. (26), obtained by analogy with a limiting reactant conversion in a cascade of CSTRs. In this case,

the base grade-efficiency curves per slice are considered equal for all slices, and the final efficiency has the value proposed by Mothes and Löffler [1].

$$\eta_i^{slice} = 1 - (1 - \eta_i^{final})^{1/N_{slices}} \quad (26)$$

This approach allows a more detailed study of particle collection in the gas-cyclone, allowing particles to escape along the inner vortex at any cyclone height, and particles to be collected as a function of axial distance. At the present state of development  $N_{slices}$  is a user-defined parameter. The effect of this parameter on the final predicted grade-efficiency curve will be given in Section 3.3.1.

### 2.3.2. Preprocessing and new particle constitution

The mass distribution that enters the cyclone is first converted to a particle number frequency distribution.

The model starts by calculating the mass of particles in the control volume ( $V_{cyclone}$ ) present at the beginning. The cyclone volume is calculated by:

$$V_{cyclone} = \frac{\pi D^2 H_c}{4} + \frac{\pi(H - H_c)(D^2 + DD_b + D_b^2)}{12} \quad (27)$$

Taking into account the mass concentration of particles ( $C$ ), the total mass of particles in the cyclone ( $m_{total}$ ) is given by:

$$m_{total} = V_{cyclone} \times C \quad (28)$$

In order to determine the actual number of particles of each particle size ( $n_{real,i}$ ) in the cyclone (Eq. (29)), it is necessary to consider the initial mass distribution ( $f_{w,i}$ ), the average diameter of each class ( $d_p$ ) and the particles' specific gravity ( $\rho_p$ ), either assuming that particles are spherical and non-porous or that the size distribution is a Stokesian distribution.

$$n_{real,i} = \frac{f_{w,i} m_{total}}{\pi d_{p,i}^3 \rho_p / 6} \quad (29)$$

At this stage, due to the very high number of particles inside the gas-cyclone, to avoid CPU and memory insufficiency, two simplifications were introduced. Maintaining the proportion among classes, the number in each size class ( $n_{original,i}$ ) which will be used in the calculations is obtained assigning a single particle to the class with the smallest number of particles. In mathematical terms, this transformation is given by Eq. (30).

$$n_{original,i} = \frac{n_{real,i}}{\min(n_{real,i}; i = 1 \dots N_{classes})}, i = 1 \dots N_{classes} \quad (30)$$

With the original number, and using Eq. (31) the relative number distribution is determined.

$$f_{n,i} = \frac{n_{real,i}}{\sum_{i=1}^{N_{classes}} (n_{real,i})} \quad (31)$$

The second simplification is introduced at this stage in order to further decrease the number of particles. Two different strategies are possible:

- To define the maximum injected diameter in the control volume (defined here as the cut-off diameter belonging to  $d_{trun}$  class);
- To define the number of representative particles through a random sampling.

Considering the cut-off diameter, the number of particles of each class to be injected in the control volume ( $n_{injected,i}$ ) is determined by Eq. (32).

$$n_{injected,i} = \frac{n_{real,i}}{n_{real,d_{trun}}} \quad (32)$$

Considering the second approach, i.e., the number of representative particles being sampled from the original distribution, several number distributions can be generated according to random sampling of the original number distribution. Both strategies are equivalent provided the cut-off diameter or the total number of sampled particles is not too small.

Regardless of which strategy is followed, it is necessary to adapt the control volume in order to maintain the ratio of volumes of particles per volume of gas actually present at the cyclone entry. This is achieved by calculating the original ratio ( $\alpha$ ) between the fluid and particle volumes (Eq. (33)), and next calculating the updated control volume using Eq. (34).

$$\alpha = \frac{V_{fluid}}{V_{particles}} = \frac{C}{\rho_p} \quad (33)$$

$$V_{control} = \frac{V_{particles,injected}}{\alpha} = \frac{\sum_{i=1}^{N_{classes}} (\pi)/(6) n_{injected,i} d_{p,i}^3}{\alpha} \quad (34)$$

As an example of this procedures, Table 2 presents the results for one case, with a mass concentration of 500 mg m<sup>-3</sup> and a cut-off diameter of 3.5 μm.

To allow for a direct comparison between the predicted grade-efficiency curves with and without agglomeration, after the agglomeration process all the formed agglomerates are assigned to existing class diameters of the original particle size distribution (PSD) histogram on a mass basis.

### 2.3.3. History reconstruction and final efficiency estimation

The core of PACyc consists in the ability of backtracking the evolution of each particle along the gas-cyclone, and to follow each particle from the early-injected particles until the final agglomerates.

Considering the gray area presented in Fig. 3, it is assumed that the agglomeration is a process that occurs along the cyclone, having a cumulative effect on the increase in the particles' sizes. In the defined interface areas (slices), there is particle removal (at the cyclone walls) and escape (at the inner vortex) obtaining a new grade-efficiency curve for each slice. The purpose of this section is to explain in detail the process of obtaining these new grade efficiency curves.

Along the simulation, several files store relevant information on the reconstruction of the history of each particle, on the new diameters formed and on the identification of each of the newly formed agglomerates.

Considering the example of two particles of class 1 (any diameter can in principle be class 1) colliding and forming an agglomerate, this agglomerate has a diameter that most probably does not exist in the initial number distribution. The newly created diameter is then identified as belonging to an ( $n + 1$ )th size (where  $n$  is the num-

**Table 2**  
Example of discretization of results after pre-processing.

D (μm)	fw %	fn %	$n_{real}$	$n_{original}$	$n_{injected}$ cuf-off	$n_{injected}$ random
0.115	0.60	84.641	6.5E+11	314,026	1154	1134
0.265	0.24	2.767	2.1E+10	10,265	37	43
0.350	0.33	1.651	1.2E+10	6126	22	27
0.450	0.69	1.624	1.2E+10	6027	22	20
0.575	3.44	3.882	2.9E+10	14,403	52	55
0.725	1.71	0.963	7.4E+09	3571	13	19
0.900	4.34	1.277	9.8E+09	4738	17	15
1.250	16.80	1.845	1.4E+10	6846	25	27
1.750	20.55	0.823	6.3E+09	3052	11	9
2.500	32.40	0.445	3.4E+09	1650	6	6
3.500	14.70	0.073	5.6E+08	272	1	1
4.500	3.67	0.009	6.6E+07	32	0	0
7.500	0.53	0.000	2.0E+06	1	0	0

**Table 3**  
Generation of some of the first diameters.

Order of generated diameter	ID of generated diameter	Particle A	Particle B
1	14	1	1
2	15	1	2
3	16	1	5
...	...	...	...
18	31	4	8

**Table 4**  
Examples of ternary and quaternary collisions.

Order of generated diameter	ID of generated diameter	Particle A	Particle B
107	120	1	14
108	121	14	31

ber of initial diameters of the original histogram). From this point on, any agglomerate resulting from the combination of two class 1 particles will lead to an agglomerate belonging to this  $(n + 1)$ th diameter.

Table 3 presents an example of information stored in this file, showing the creation of diameter 14 as a result of the agglomeration of two particles of class 1, the creation of diameter 15 (resulting of the agglomeration of one particle of class 1 and one class 2), the formation of diameter 16 (resulting of the agglomeration of one particle of class 1 and one class 5) and finally the creation of diameter 31 as a result of agglomeration of a particle of class 4 and one of class 8.

All these results consider only the possibility of binary interactions of two original particles (particles with diameter equal to the mean diameter of each class). However, the agglomeration model leads indirectly to higher order particle interaction, as presented in Table 4, where two other types of binary combinations are shown: original particles with agglomerates and agglomerates with agglomerates.

In these cases, diameter 120 is achieved when a particle diameter of class 1 agglomerates with a previously formed agglomerate (with a diameter identified as 14). As presented in the previous example, diameter 14 consists of two particles of class 1. Therefore, we conclude that diameter 120 results from the combination

**Table 5**  
Diameter constitution.

ID	Initial classes												
	1	2	3	4	5	6	7	8	9	10	11	12	13
Initial classes													
1	1	-	-	-	-	-	-	-	-	-	-	-	-
2	-	1	-	-	-	-	-	-	-	-	-	-	-
3	-	-	1	-	-	-	-	-	-	-	-	-	-
4	-	-	-	1	-	-	-	-	-	-	-	-	-
5	-	-	-	-	1	-	-	-	-	-	-	-	-
6	-	-	-	-	-	1	-	-	-	-	-	-	-
7	-	-	-	-	-	-	1	-	-	-	-	-	-
8	-	-	-	-	-	-	-	1	-	-	-	-	-
9	-	-	-	-	-	-	-	-	1	-	-	-	-
10	-	-	-	-	-	-	-	-	-	1	-	-	-
11	-	-	-	-	-	-	-	-	-	-	1	-	-
12	-	-	-	-	-	-	-	-	-	-	-	1	-
13	-	-	-	-	-	-	-	-	-	-	-	-	1
Formed agglomerates													
14	2	-	-	-	-	-	-	-	-	-	-	-	-
15	1	1	-	-	-	-	-	-	-	-	-	-	-
16	1	-	-	1	-	-	-	-	-	-	-	-	-
17	1	-	-	-	-	-	-	-	-	-	1	-	-
...	...	...	...	...	...	...	...	...	...	...	...	...	...
31	-	-	-	1	-	-	-	1	-	-	-	-	-
...	...	...	...	...	...	...	...	...	...	...	...	...	...
120	3	-	-	-	-	-	-	-	-	-	-	-	-
121	2	-	-	1	-	-	-	1	-	-	-	-	-

of 3 particles of class 1. This particle may be interpreted as an agglomerate formed by a ternary collision process.

Another example of combination at higher level is the formation of an agglomerate of diameter 121, which is achieved when an agglomerate of diameter 14 joins an agglomerate of diameter 31. Since diameter 14 consists of two particles of class 1 and diameter 31 consists of a particle of class 4 and another of class 8, we conclude that diameter 121 is obtained through the agglomeration of 4 original particles, two of class 1, one of class 4 and another of class 8. This particle may thus be interpreted as an agglomerate formed by a quaternary collision process.

The model leads to combinations of much higher level, and it is possible, with times of interaction of the order of several seconds, that agglomeration of all particles in one single agglomerate may occur. Our approach prevents this to happen, not only because the interaction times are usually below 1 second, but also because particles are removed along the axial axis of the cyclone both at the inner vortex and at the cyclone walls, becoming unavailable for further agglomeration.

With the stored information, a database is built with each diameter. Table 5 presents this matrix structure, which reflects the formation of each diameter (existing or newly created) as a function of available mass classes. In the matrix each column corresponds to an existing class (in the example shown, 13 columns) and each line corresponds to a diameter, original or created (the first 13 rows correspond to pre-existing original diameters while the other correspond to newly created diameters).

Each new particle is recorded as shown in Table 6. The major difference between Table 3 (or Table 4) and Table 6 is that this last table stores the real number of particles created. It is possible to refer that both lines 2 and 104 of column 1 of Table 6, produce particles of diameter 15 (column 4), while lines 3, 4 and 101 produce particles of diameter 16.

The class grade-efficiency curve is obtained weighting each diameter collection efficiency, using the model proposed by Mothes and Löffler [1], as it will be presented in detail below. Table 7 shows the diameters of the particles and the corresponding collection efficiencies.

Cross-referencing Tables 3, 4 and 7 it is possible to draw some conclusions about each diameter collection efficiency, e.g.:

**Table 6**  
Logging the generation of each new diameter.

Order of formed agglomerate	Particle A	Particle B	Agglomerate diameter ID
1	1	1	14
2	1	2	15
3	1	5	16
4	1	5	16
5	1	11	17
...	...	...	...
101	1	5	16
102	7	9	39
103	3	7	40
104	1	2	15
105	1	8	20

**Table 7**  
Diameter of each particle and corresponding removal-efficiency (per slice).

Diameter ID	Diameter (μm)	Collection Efficiency (%)
Initial classes		
1	0.115	0.034
2	0.265	0.077
3	0.350	0.112
4	0.450	0.165
5	0.575	0.250
6	0.725	0.384
7	0.900	0.584
8	1.250	1.165
9	1.750	2.616
10	2.500	6.614
11	3.500	10.961
12	4.500	14.364
13	7.500	21.670
Formed agglomerates		
14	0.145	0.042
15	0.272	0.080
16	0.577	0.252
17	3.500	10.961
...	...	...
31	1.269	1.205
...	...	...
120	0.167	0.047
121	1.270	1.207

- Original particle case: the diameter identified as 1 corresponds to a diameter of  $1.15 \times 10^{-7}$  meter with an efficiency of  $\approx 3.44 \times 10^{-4}$  and consists of a particle of diameter belonging to class 1;
- Binary particle case: the diameter identified as 31 corresponds to a diameter of  $\approx 1.27 \times 10^{-6}$  meter with an efficiency of  $\approx 1.21 \times 10^{-2}$  and consists of one particle of diameter belonging to class 4 and another to class 8;
- Ternary particle: the diameter identified as 120 is a diameter of  $\approx 1.67 \times 10^{-7}$  meter with an efficiency of  $\approx 4.72 \times 10^{-4}$  and is composed by three particles belonging to class 1;
- Quaternary particle case: the diameter identified as 121, corresponds a diameter of  $\approx 1.27 \times 10^{-6}$  meter with an efficiency of  $\approx 1.21 \times 10^{-2}$  and consists of two particles of class 1, one of class 4 and another of class 8;

At this stage, we emphasize the fact that particles with diameters 31 and 121, in spite of being composed by different sized particles, have very similar collection efficiencies. This has great impact on the grade-efficiency curves. Although diameter 121 has two particles of class 1 in its constitution, these have in fact a collection efficiency very close to the collection efficiency of an isolated particle class 8 or the combination of a particle class 4 and a particle class 8, since they belong to similar sized agglomerates.

To calculate the collection efficiency per slice, the cyclone is considered as a cascade of separation units, much as it is done with

the yield of reaction in a cascade of chemical reactors, as has been referred before. This is shown in Eq. (26), which allows to estimate the reference slice efficiency, using the efficiency calculated by the Mothes and Löffler model [1] for gas cyclones. Thus, the efficiency of each diameter in each slice ( $\eta_i^{slice}$ ) is obtained using the final efficiency of each diameter ( $\eta_i^{final}$ ) and the number of slices ( $N_{slices}$ ).

By combining the information of the creation of each diameter and the creation of each particle, a INFO matrix saves the information of the final location of each particle diameter in each of the (existing or created) diameters. This structure identifies the number of particles of diameter  $i$  that behave like particles of diameter  $j$ . As a summary of the information stored in this matrix, it is possible to refer that:

- The number of lines is equal to the number of original classes;
- The number of columns is the sum of the number of the created diameters and the number of classes;
- The sum per line is equal to the initial number of particles of each class.

Combining the INFO matrix with the correspondent collection efficiency, the final efficiency is obtained weighting the number of particles  $j$  that behave as  $i$  particles. An expression that translates this relation is given in Eq. (35), where  $\eta_i^{final,*}$  is the final efficiency after agglomeration of a particle belonging to diameter of class  $i$ , INFO is a structure with all information about the  $i$  particles that shifted to class  $j$ ,  $\eta_j^{slice}$  is the efficiency of each  $j$  diameter,  $n_{i,j}$  is the number of particles  $i$  in class  $j$ ,  $D_{initial,i}$  and  $D_{final,i}$  are respectively the smallest and the largest diameters that belong to class  $i$  and  $N_{classes}$  is the original number of classes.

$$\eta_i^{final,*} = \frac{\sum_{j=D_{initial}}^{D_{final}} INFO_{i,j} \times \eta_j^{slice}}{\sum_{j=D_{initial}}^{D_{final}} n_{i,j}}, \quad i = 1 \dots N_{classes} \quad (35)$$

In Fig. 5 the agglomeration process is schematically represented. This figure shows the evolution of the relative number of particles in each class along the agglomeration/removal process, thus, as a function of elapsed contact time. In the beginning, all particles (100%) are in their respective class (viz the matrix diagonal).

Some of the major conclusions of Fig. 5 are as following:

- As the agglomeration proceeds, the particles shift towards larger diameters (to the right) and particle removal along the gas cyclone can be observed, because the total blue area (particle number fraction of each initial class) decreases and the red area (corresponding to the particles that escape or are collected in the cyclone) increases with time.
- Not even after a long elapsed time, all particles belonging to class 1 shift to larger classes. This is due to the fact that, usually, the number frequency of the smaller particles is very high, and even though the majority of the particles shift to larger classes, some particles remain in their respective class.
- Classes 8–10 have predominance at the final interaction time. This is due to the shape of the baseline grade-efficiency curve, as classes larger than 11 are completely captured and the finer classes shift towards larger classes. As classes 8–10 have intermediate collection efficiencies, particles belonging to these classes remain longer in the control volume;
- Particles belonging to the largest class (class 12), as time elapses, are being removed from the control volume, because this class has complete collection.

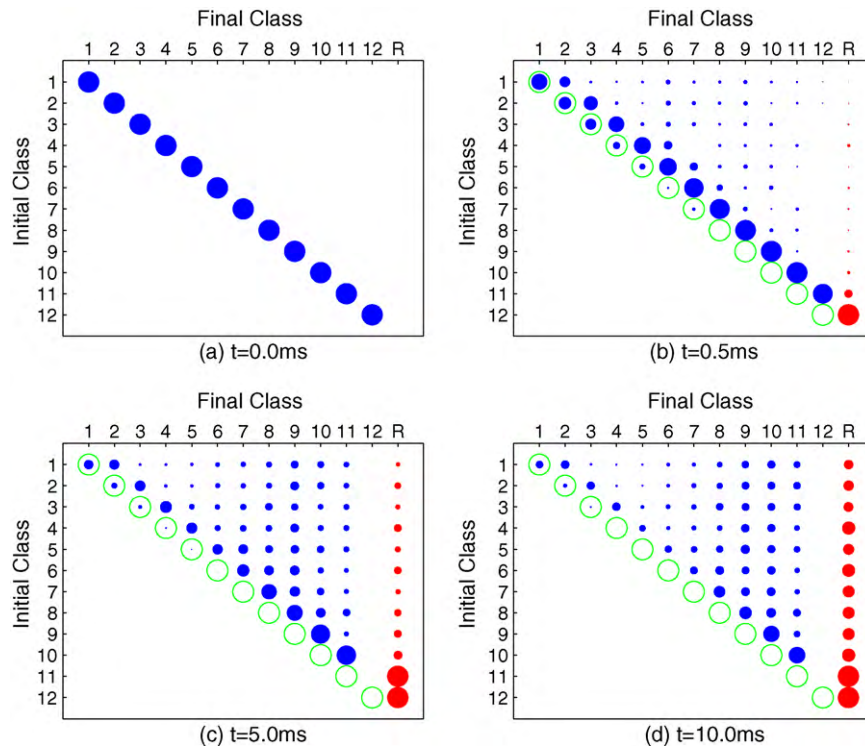


Fig. 5. Proportion of each diameter in each of the initial classes (matrix representation) ( $u = 12 \text{ m s}^{-1}$ ,  $\rho = 1500 \text{ kg m}^{-3}$ ,  $c = 1 \text{ g m}^{-3}$ , 20 slices, random sampling of 10k particles).

### 3. Results and discussion

This section shows several results obtained with the PACyc model while simulating a case study. Initial and final mass and number distributions are shown in Section 3.2, and two key elements of PACyc are compared: continuous vs. discrete control volume and random sampling vs. cut-off diameter.

A sensitivity study was made considering some major parameters and their impact on the predicted grade-efficiency curves. Finally, model predictions are compared with preliminary experimental data obtained at pilot-scale.

#### 3.1. Model intermediate results

To better understand the final results obtained by the PACyc model, some intermediate results are shown.

To calculate the probability of collision between two particles it is necessary to estimate their trajectories and their velocity components. Keeping in mind that the collisions are defined by a probabilistic criteria, in order to better picture the agglomeration of two different sized particles, Fig. 6 shows three particles' trajectories: the downward trajectory is from a particle of  $0.26 \mu\text{m}$  and the upward trajectory is from a particle with  $5 \mu\text{m}$ . These trajectories are the direct result of solving Eqs. (4)–(15), in a 3D framework, so that collisions can be better visualized.

The trajectory of the smaller particle (B) is much more random than that of the larger particle (A), and after agglomeration, the trajectory of agglomerate (C) is similar to that of the larger particle. It is visible that the smaller particles are more affected by the turbulent flow field than the larger particles. As the trajectory of this new agglomerate is calculated solving the momentum equations, the resulting particle has a tendency to follow the trajectory of the larger particle.

Fig. 7 presents the simplification introduced when two particles agglomerate. The new particle diameter is determined considering mass conservation of the particles. It should be stated that this

simplification may introduce a large error in the equivalent aerodynamic diameter of the resulting agglomerate, whenever similar sized particles collide and agglomerate. Fortunately, the frequency of collisions for similar-sized particles is very low because of the small relative velocities. Lipowsky and Sommerfeld [23] have proposed a model for agglomerate porosity, but this is yet to be experimentally validated.

#### 3.2. PSD analysis

The mass distribution is an input to the model. The model converts the information stored in this distribution to a number distribution, assuming that particles are spherical. Thus, particle size distributions based on Stokes' law should be employed whenever feasible.

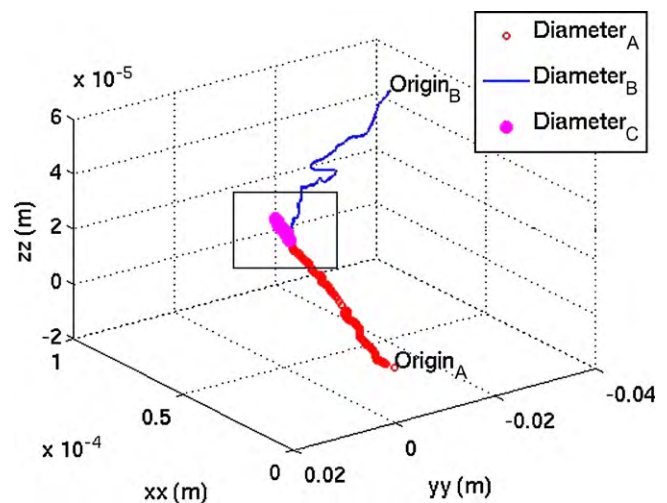


Fig. 6. Pseudo-realistic visualization of trajectories and agglomeration effect in two particles.

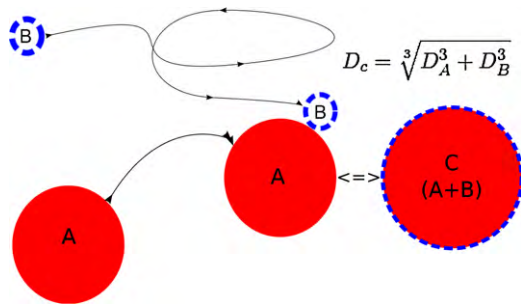


Fig. 7. New diameter calculation.

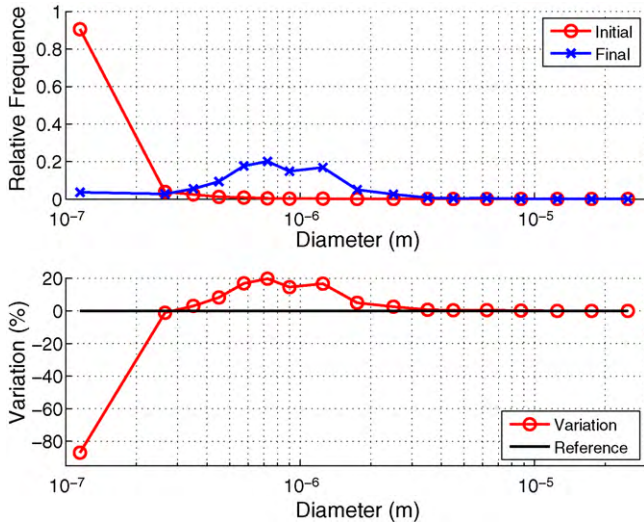


Fig. 8. Initial and final number distribution ( $u = 12 \text{ m s}^{-1}$ ,  $\rho = 1500 \text{ kg m}^{-3}$ ,  $c = 1 \text{ g m}^{-3}$ ).

After studying the agglomeration impact on the grade-efficiency curves, the model calculates the final number distribution and recalculates the corresponding mass distribution. Figs. 8 and 9 show the initial and final number and mass distributions before and after particle interaction/agglomeration.

Fig. 8 shows a clear reduction in the number of smaller particles and the correspondent increase in the number of the following classes. In the number distribution the positive shift to the larger

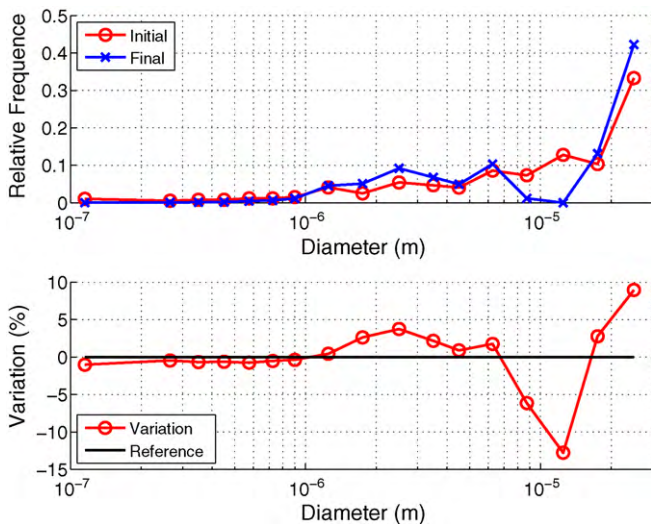


Fig. 9. Initial and final mass distribution ( $u = 12 \text{ m s}^{-1}$ ,  $\rho = 1500 \text{ kg m}^{-3}$ ,  $c = 1 \text{ g m}^{-3}$ ).

particles is not visible, hence the presentation of the correspondent mass distribution in Fig. 9.

Fig. 9 shows that the modal class in the beginning corresponds to the first class (corresponding to a diameter around  $25 \mu\text{m}$ ). Analyzing the result of the model, there is a displacement of the finer particles (below  $1 \mu\text{m}$ ) to larger diameters, and there is also a displacement of the particles around  $10 \mu\text{m}$  to larger diameters. This shows that the smaller particles are disappearing (the variation of the first seven classes is negative) and that there is formation of larger particles (the variation of the next six classes is positive).

Fig. 9 also shows that particle diameters around  $10 \mu\text{m}$  tend to increase in size towards  $17$  and  $25 \mu\text{m}$  sizes. One possible reason for this is that if there are only a few particles of the larger diameters, as it may happen due to sampling (Section 3.3.2), these particles upon colliding with smaller particles may jump to a larger class diameter, justifying the negative class variation just before the corresponding positive class variation of the larger classes.

### 3.3. Grade-efficiency curves

In this section we present some results obtained using the proposed model. All the simulations were performed with the cyclone geometry proposed by Salcedo and Cândido [17], with internal diameter =  $740 \text{ mm}$  and inlet mean velocity of  $20 \text{ m/s}$ , without partial recirculation of gases and particles. The radial turbulent dispersion coefficient was considered constant ( $D_r = 1.27 \times 10^{-2} \text{ m}^2/\text{s}$ ) as obtained by Salcedo and Coelho [5], the temperature was  $313 \text{ K}$  and the absolute pressure was  $953 \text{ mBar}$ .

For all the cases in this section, the model baseline case has an efficiency curve obtained by the Mothes and Löffler model [1], and the sample has a specific gravity of  $1500 \text{ kg m}^{-3}$  and inlet concentration of  $1 \text{ g m}^{-3}$ .

For discretization, 17 diameters between  $0.12$  and  $25 \mu\text{m}$  were considered, as a compromise to have several (7) submicrometric classes but still large particles for acting as targets. These are the mean class diameters that correspond to a GRIMM 1.108 laser spectrometer, employed in one of the experimental runs (Section 3.4) and proved to be adequate for performing simulations in reasonable time.

#### 3.3.1. Control volume: continuous vs. discrete

Two key elements of PACyc (and correspondent different approaches) were studied: the control volume (continuous vs. discrete) and the number sampling method (cut-off diameter vs. random sampling).

The control volume has an annular geometry, because it is confined between the outer diameter of the vortex finder and the inner diameter of the volume-equivalent cylindrical body.

Considering the definition of continuous control volume, PACyc handles it as a single slice, with a residence time equal to the average residence time of the gas, and with particle removal occurring only at the end of the slice.

The discrete cases are defined by the correspondent number of slices, with each slice having the same residence time, equal to the cyclone residence time divided by the number of slices. Between two consecutive slices, there is particle removal.

Fig. 10 shows the impact on efficiency of the number of slices. Considering the continuous control volume (1 slice), the grade-efficiency curve is the lowest. This fact was taken into account to make conservative forecasts of overall efficiencies as given in Section 3.4.

With the number of slices increasing to 40, the grade-efficiency increases as well. From 40 to 100 slices the grade-efficiency decreases, and the systems represented by 5 or by 100 slices have almost the same predicted grade-efficiency curves.

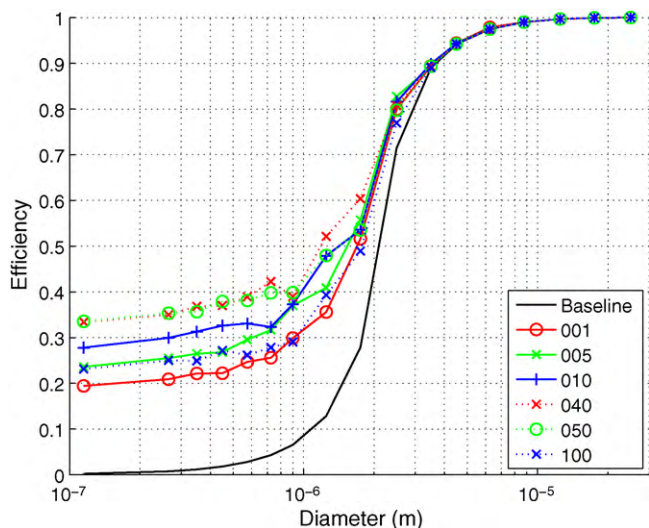


Fig. 10. Sensitivity analysis discrete control volume—number of slices.

This parameter has a mixed effect on the final grade–efficiency curves, being justifiable by two opposing effects, as explained below.

In the case with only one slice (viz, the continuous control volume), there is no particle removal along the cyclone. All particles are initially inside the cyclone but this does not mean that they are available to collide in the control volume, since PACyc considers that when particles collide with the cyclone wall, they are no longer available to agglomerate (a zero probability of collision is assigned to these particles). PACyc also considers that particles that reach the vortex finder are lost and exit the cyclone.

In the case with several slices, considering that in the beginning of each slice all remaining particles are injected in an annular surface, the normal path of the particles is towards the cyclone wall, eventually preventing further agglomeration. The frontier between slices has the impact of randomly repositioning (reinjecting) the particles further apart from the cyclone wall, transforming particles that were unavailable to agglomerate in the current slice into particles available to agglomerate in the next slice. Thus, complete back mixing is assumed when crossing from one slice to the next.

As the number of slices increases, the particles are more and more available to agglomerate, because they are being consecutively reinjected in the annular surface. However, there is also increased particle removal along the cyclone (between slices). These two factors work one against the other, with the consequence that there exists some intermediate number of slices that show the maximum grade–efficiencies (in this case, around 40–50 slices).

### 3.3.2. Number distribution sampling: cut-off diameter vs. random sampling

There are two strategies of sampling available in the PACyc model to generate the number particle size distribution to be processed by the model. In the cut-off diameter strategy, a single particle is assigned to the correspondent diameter and the number frequency for smaller sizes are generated by maintaining the correct proportions of the original number distribution. In this case study, a cut-off diameter of 8  $\mu\text{m}$  corresponds approximately to 20k particles, a cut-off of 12  $\mu\text{m}$  to 70k particles, and a cut-off of 17  $\mu\text{m}$  to 120 k particles. Figs. 11 and 12 show the simulation results obtained.

Fig. 11 shows the influence of the cut-off diameter on the grade–efficiency curves. This parameter determines directly the initial largest diameter available for collision and as this parameter increases, higher efficiencies are obtained for the smaller particles.

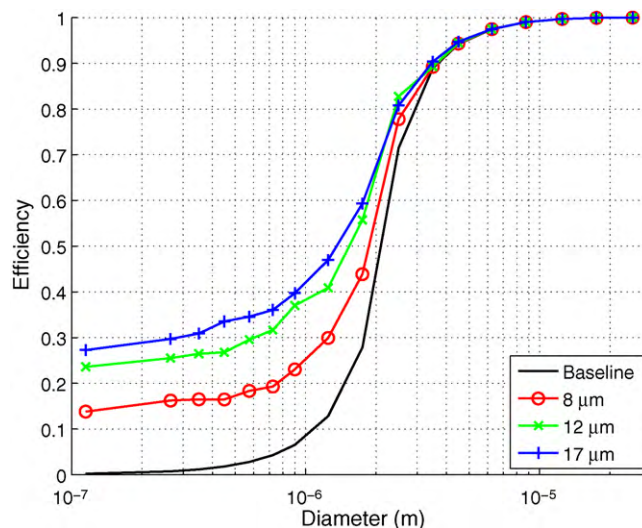


Fig. 11. Sensitivity analysis—cut-off diameter (with 5 slices).

Obviously, choosing a small value for the cut-off diameter biases the results towards less agglomeration, because the larger particles (that are mainly target particles) are either absent or present in very small numbers. As the cut-off diameter is increased, more larger particles are present to interact, and injecting more larger particles implies that there are more target particles available, with collection efficiencies around 100% to collect the smaller ones.

Fig. 12 presents the corresponding cases using the random sampling method. It is shown that this method predicts higher grade–efficiency curves for the smaller number of particles than the correspondent cut-off cases. Only the cases of 17  $\mu\text{m}$  vs. 120k particles have almost the same efficiency curves, allowing to consider that similar results are obtained with either a high cut-off or a large number of sampled particles. This has been confirmed with several different simulations.

Fig. 12 shows that the grade–efficiency curves with 120k particles are actually lower than with 70k particles. With this sampling method, using a single sample, it is impossible to draw conclusions about the impact of the number of particles on the final grade–efficiency curves. Thus, a statistical average should be used, but with the negative effect of increased CPU effort.

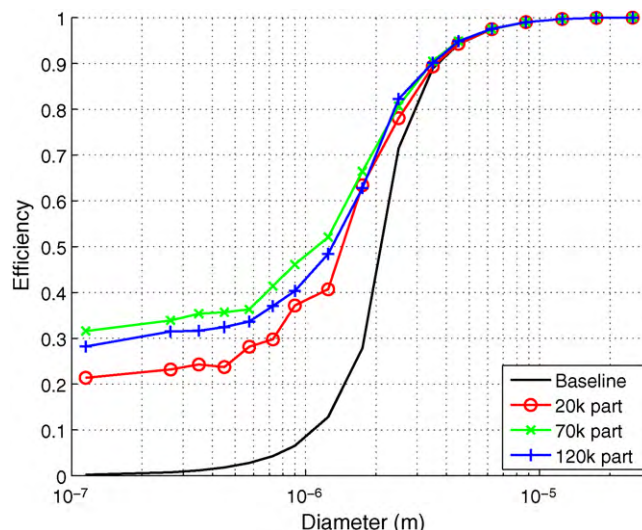


Fig. 12. Sensitivity analysis—random sampling (with 5 slices).

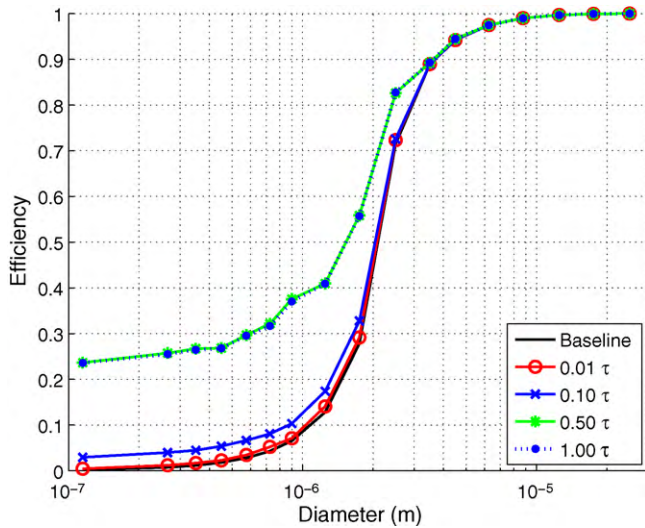


Fig. 13. Sensitivity analysis discrete control volume–interaction time.

Increasing the number of sampled particles beyond 200–500k does not bring any significant change in the predicted grade-efficiency curves. This fact was taken into account to make forecasts within reasonable CPU times as given in Section 3.4.

3.3.3. Sensitivity analysis: interaction time

For the specific gravity sensitivity analysis, the Mothes and Löffler baseline grade-efficiency curves [1] will be presented individually.

For the cases with agglomeration, the reference case adopts the following values for the parameters studied: time of interaction ( $1\tau = 0.7\text{ s}$ ), sampling method (cut-off diameter  $12\ \mu\text{m}$ ) and control volume (discrete with 5 slices).

Fig. 13 presents the impact of the interaction time on the final grade-efficiency curves.

This parameters has an asymptotic behavior, justified by the fact of particles hitting the cyclone wall before the residence time is reached, becoming unavailable for agglomeration. Prior to the moment of all particles hitting the wall, it is possible to observe that as the residence time of the gas increases higher efficiencies are obtained for the smaller particles. After all the particles hit the wall (in this case  $t \geq 0.5\tau$ ), the final grade-efficiency is the same and independent of the residence time.

3.3.4. Sensitivity analysis: specific gravity

Fig. 14 presents the initial efficiency without agglomeration, and the grade-efficiencies obtained by varying the particle specific gravity.

The predicted grade-efficiencies increase with specific gravity as expected. In terms of agglomeration, the agglomeration model leads to higher efficiencies as this parameter is increased, due to the initially higher baseline efficiency for the larger particles, which act as targets for the finer ones.

3.3.5. Sensitivity analysis: concentration

Fig. 15 presents the final grade efficiency curves as inlet concentration increases.

At very low concentrations, collision and agglomeration are two phenomena with almost no significance due to the small number of particles present in the control volume. However, even for low concentrations ( $100\ \text{mg m}^{-3}$ ) this model predicts grade-efficiency curves higher than those initially predicted by Mothes and Löffler [1]. On the other hand, for larger concentrations, the agglomeration phenomenon has increasing relevance, so the final efficiency for the smaller particles increases substantially over the base-case.

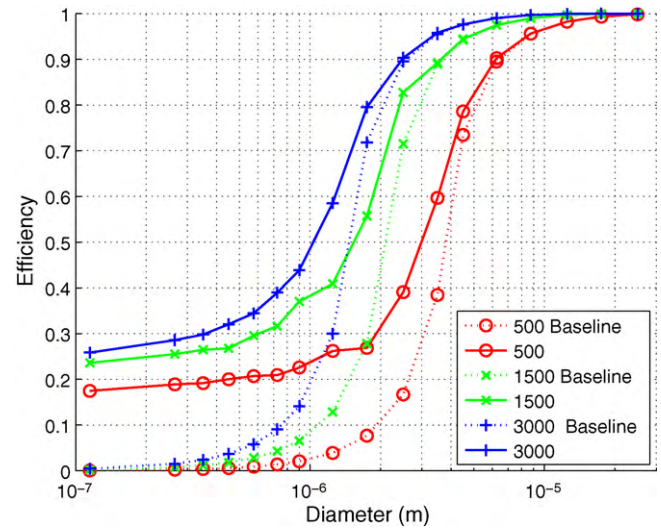


Fig. 14. Sensitivity analysis discrete control volume-specific gravity.

3.4. Experimental results and model prediction

In this section we present experimental results for 2 case studies, and compare them with PACyc predictions.

Figs. 16 and 17 show two cumulative particle size distributions, respectively for the feed and cyclone emissions. In both, the circles correspond to the off-line measurements using a Coulter LS230 laser sizer of calcined mineral powder and the diamonds correspond to online measurements of a GRIMM 1.108 laser sizer for the same sample ( $\rho_p = 2700\ \text{kg m}^{-3}$ , inlet concentration =  $1.28\ \text{g m}^{-3}$ ). The crosses correspond to the Coulter measurements of a sulfanilic acid sample ( $\rho_p = 1450\ \text{kg m}^{-3}$ , inlet concentration =  $7.7\ \text{g m}^{-3}$ ) [19].

Figs. 18 and 19 present a comparison between PACyc predictions and actual experiments for both powders. The simulation results presented are the average ( $\pm 95\%$  confidence interval) of ten runs using different seeds to generate all the pseudo random numbers used by the model. All runs were made considering a continuous control volume (viz. one slice), random sampling of 200k particles and interaction time defined by the cyclone volume and operating conditions.

In both cases, a pilot numerically optimized cyclone [8,17] with internal diameter of 450 mm without partial recirculation of gases

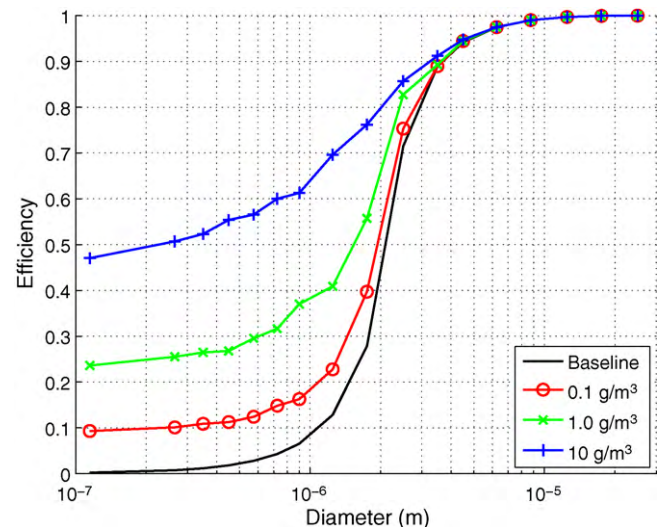


Fig. 15. Sensitivity analysis discrete control volume–concentration.

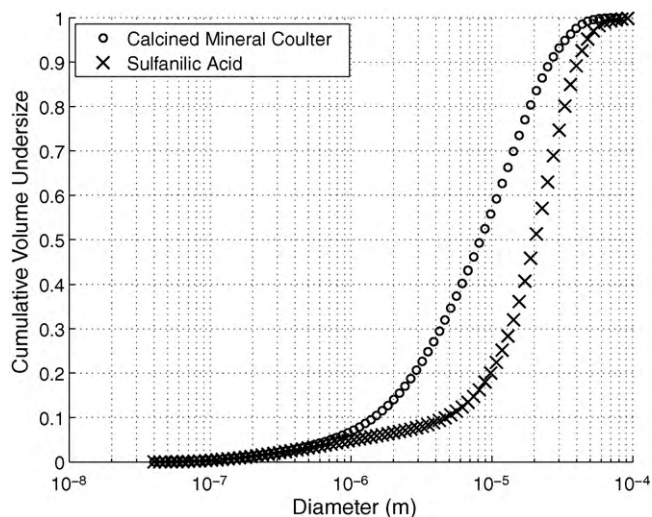


Fig. 16. Volume distributions in feed.

and particles was used. For the sulfanilic acid powder, the pilot cyclone was actually fitted on a test rig at the industrial site, thus no particle feeder was employed. For the calcined mineral experiment, a TOPAS 410G particle feeder was employed.

The experimental grade-efficiency curves were obtained with simultaneous inlet/outlet isokinetic sampling using constant volume samplers (Techora Bravo), in GFA glass fiber filters. Particle size distributions were measured off-line with the Coulter, with ultrasound dispersion in appropriate liquid media. For the calcined mineral experiments, online measurements of emissions were also done using the GRIMM laser spectrometer.

For the calcined mineral powder the inlet mean velocity was  $\approx 20 \text{ m s}^{-1}$ , while for the sulfanilic acid it was  $\approx 15 \text{ m s}^{-1}$ .

Table 8 presents the experimental overall collection efficiencies for the cases shown in Figs. 18 and 19, and it is possible to conclude that PACyc predicts better the experimental overall efficiency than the Mothes and Löffler [1] model for these two cases.

Fig. 20 compares the global collection efficiencies experimentally obtained with the predicted from the PACyc model.

Superimposed in Fig. 20 is the model proposed by Smolik (as quoted by Svarovsky [28]) to predict global efficiency for an unknown concentration ( $c_2$ ), knowing the efficiency at a lower value ( $c_1$ ), as given by Eq. (36). The empirical constant proposed by Smolik is  $k = 0.18$ , clearly overpredicting the overall efficiency of

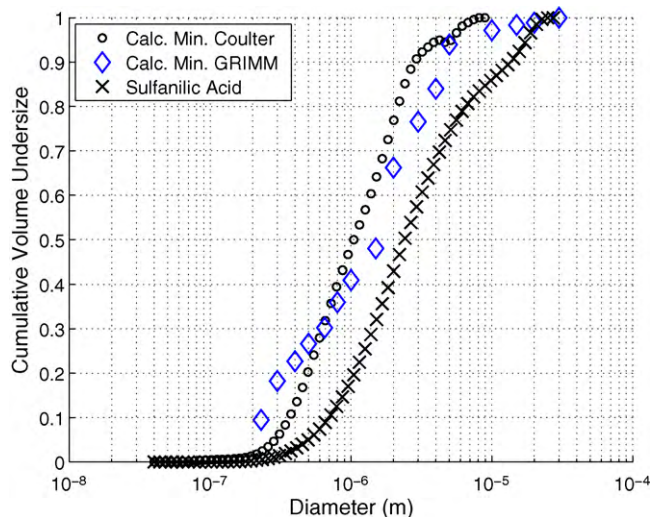


Fig. 17. Volume distributions in emissions.

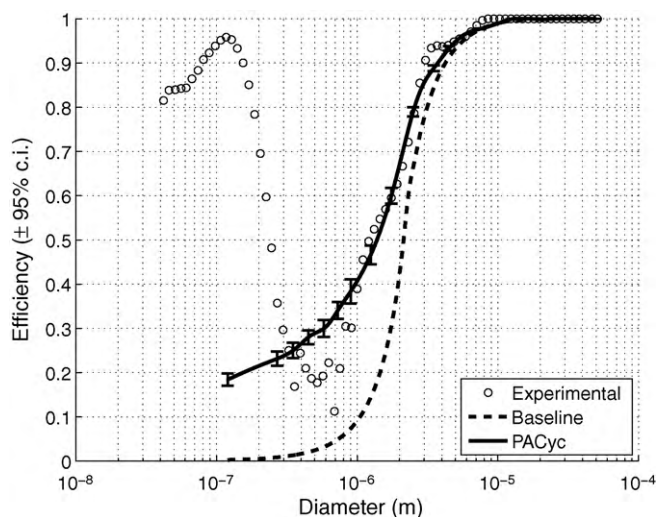


Fig. 18. Experimental results and PACyc's predictions—calcined mineral powder.

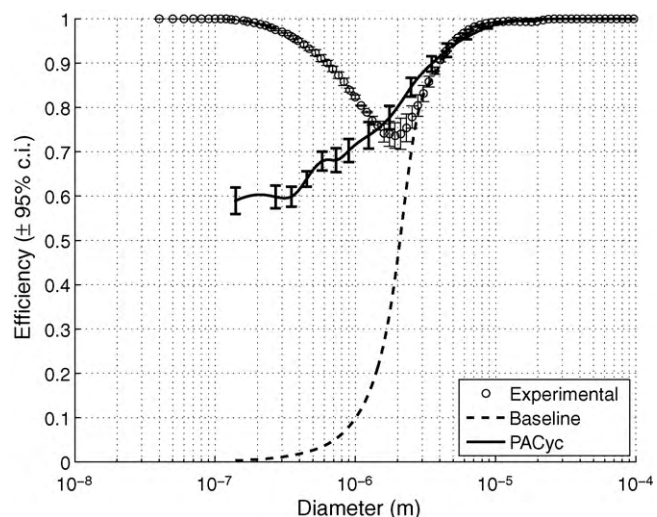


Fig. 19. Experimental results and PACyc's predictions—sulfanilic acid.

the higher concentration cases. For the calcined mineral studied in this experiment, this low concentration experiment was made at  $c_1 = 56.5 \text{ mg m}^{-3}$  corresponding to an overall collection efficiency of  $\eta(c_1) = 87.0\%$  and the value of  $k$  that fits best the experimental data was about  $k = 0.0887$ , meaning that this dust agglomerates to a lower degree than expected from the Smolik experimental exponent.

$$\eta(c_2) = 1 - (1 - \eta(c_1)) \left( \frac{c_1}{c_2} \right)^k \quad (36)$$

Since the Mothes and Löffler model does not take feed powder concentration into account, it underpredicts collection, a fact that has been shown before at both laboratory and industrial scales [2,9].

Table 8  
Overall collection efficiencies.

Case	Mothes and Löffler (%) [1]	PACyc (%)	Experimental (%)
Calcined mineral	83.6	88.6 ± 0.4	89.9
Sulfanilic acid	92.1	96.5 ± 0.2	98.5 ± 0.2

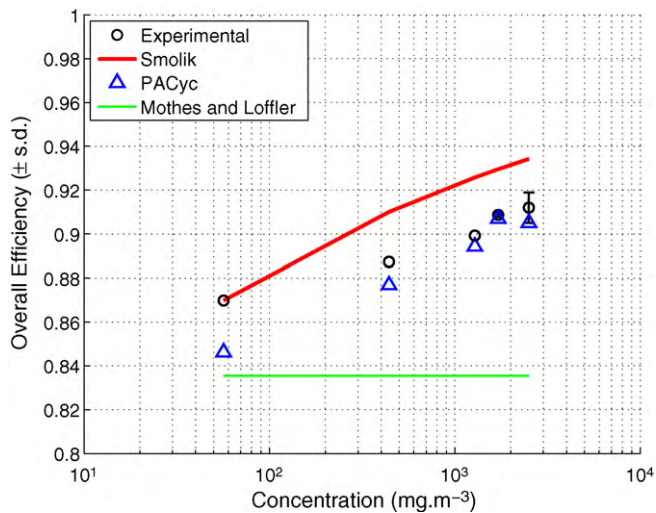


Fig. 20. Overall efficiencies—calcined mineral case.

Considering the grade-efficiency curves, Figs. 18 and 19 show that the PACyc model predicts reasonably well the experimental data, although clearly under predicting efficiencies below  $\approx 1 \mu\text{m}$ . It is possible to observe that for the mineral powder (Fig. 18), the under predictions are for particles smaller than  $\approx 0.3 \mu\text{m}$ , while for the sulfanilic acid (Fig. 19), the under predictions are for particles smaller than  $\approx 1.5 \mu\text{m}$ . For the sulfanilic case, two experiments were made at the same inlet conditions, and it is possible to conclude that the cyclone has reproducible collection efficiencies.

The model cannot, however, predict the hook-like shape grade-efficiency curves experimentally observed for these two cases, and the probable reasons for this are that:

- for realistic particle size distributions, such as those used in this work, there is CPU/memory insufficiency to completely represent the distributions. For example, it can be shown for the suphanilic acid particle size distribution, that sampling 500k particles will only inject 2 particles of  $17 \mu\text{m}$  in the control volume. Ho and Sommerfeld [18] show that for particles below  $2 \mu\text{m}$  the number frequency tends to zero as the agglomeration process occurs. However, the distributions employed by these authors, unfortunately, do not correspond to realistic volume distributions as found in industrial practice;
- there is some extra mechanism responsible for agglomeration of these fine particles, such as electrostatic charging in the inlet conveying piping to the cyclone [7], which are not presently considered in the model.

#### 4. Conclusions

The PACyc model, coupling the Mothes and Löffler and the Sommerfeld models [1,15,18], leads to a better prediction of the experimental grade-efficiency curves, as well as of the overall collection.

The agglomeration phenomena seems to be a good justification of the large observed collection efficiencies obtained experimentally for fine particles using cyclones.

The agglomeration model presented in this work has some parameters which must be further studied, like the collision properties or the influence of the material under study, but at the present moment, the model can predict in qualitative (and in some cases in a quantitative) manner the increased efficiencies for submicrometric particles, a fact that has been experimentally observed by several authors [2–9].

In spite of presently disregarding the possible effect of electrical forces in promoting agglomeration of the finest particles, PACyc is an improvement of the existing models developed to predict grade-efficiency curves in gas-cyclones. It is expected that, after further characterization of the model parameters based on physical properties of the particles and the inclusion of electrical forces, theoretical results may better represent the experimental ones, allowing a more correct optimization of the design and optimization of gas-cyclones. This work is currently under development.

#### Acknowledgements

The authors would like to thank to FCT (Fundação para a Ciencia e Tecnologia) for the grant BDE/15628/2006 and for the Co-financing of the industrial partner (CUF-Quimicos Industriais S.A.).

#### References

- [1] H. Mothes, F. Löffler, Prediction of particle removal in cyclones separators, *International Chemical Engineering* 28 (1988) 231.
- [2] R.L.R. Salcedo, V.G. Chibante, A.M. Fonseca, G. Candido, Fine particle capture in biomass boilers with recirculating gas cyclones: Theory and practice, *Powder Technology* 172 (2) (2007) 89–98.
- [3] A.C. Hoffmann, A. Vansanten, R.W.K. Allen, R. Clift, Effects of geometry and solid loading on the performance of gas cyclones, *Powder Technology* 70 (1992) 83–91.
- [4] A.C. Hoffmann, A. Berrino, On the shape of grade-efficiency curves computed for centrifugal dedusters by cfd with lagrangian particle tracking, *Advanced Technologies for Fluid-Particle Systems* 95 (1999) 13–17.
- [5] R.L. Salcedo, M.A. Coelho, Turbulent dispersion coefficients in cyclone flow: An empirical approach, *Canadian Journal of Chemical Engineering* 77 (4) (1999) 609–617.
- [6] E. Hugi, L. Reh, Focus on solids strand formation improves separation performance of highly loaded circulating fluidized bed recycle cyclones, *Chemical Engineering Processing* 39 (2000) 263–273.
- [7] A.C. Hoffmann, L.E. Stein, *Gas Cyclones and Swirl Tubes—Principles, Design and Operation*, second ed., Springer, 2008.
- [8] R.L. Salcedo, M.J. Pinho, Pilot and industrial-scale experimental investigation of numerically optimized cyclones, *Industrial & Engineering Chemical Research* 42 (2003) 145–154.
- [9] V.G. Chibante, A.M. Fonseca, R.R. Salcedo, Comparison the performance of recirculating cyclones applied to the dry scrubbing of gaseous hcl with hydrated lime, *Industrial & Engineering Chemical Research* 48 (2) (2009) 1029–1035.
- [10] C.A. Ho, M. Sommerfeld, Numerische berechnung der staubabscheidung im gaszyklon unter berücksichtigung de partikelagglomeration, *Chemie Ingenieur Technik* 77 (3) (2005) 282–290.
- [11] E. Muschelkautz, W. Krambrock, Design of cyclone separators in the engineering practice, *Chemical Engineering & Technology* 42-5 (1970) 247–255.
- [12] E. Muschelkautz, M. Trefz, Design and calculation of higher and highest loaded gas cyclones, in: *Proceedings of Second World Congress on Particle Technology*, Kyoto, 1990, pp. 52–71.
- [13] E. Muschelkautz, M. Trefz, Pressure and separation efficiency in cyclones, *VDI-Warmeatlas* 6 (1991) 1–9.
- [14] H. Mothes, F. Löffler, About the influence of particle agglomeration on the separation in a gas cyclone, *Staub Reinhaltung Der Luft* 44 (1984) 9–14.
- [15] M. Sommerfeld, Validation of a stochastic lagrangian modelling approach for inter-particle collisions in homogeneous isotropic turbulence, *International Journal of Multiphase Flow* 27 (10) (2001) 1829–1858.
- [16] D. Mao, J.R. Edwards, A. Kuznetsov, R. Srivastava, A model for fine particle agglomeration in circulating fluidized bed absorbers, *Heat and Mass Transfer* 38 (2002) 379.
- [17] R.L.R. Salcedo, M.G. Candido, Global optimization of reverse-flow gas cyclones: application to small-scale cyclone design, *Separation Science and Technology* 36 (12) (2001) 2707–2731.
- [18] C.A. Ho, M. Sommerfeld, Modelling of micro-particle agglomeration in turbulent flows, *Chemical Engineering Science* 57 (15) (2002) 3073–3084.
- [19] R.L. Salcedo, Collection efficiencies and particle-size distributions from sampling cyclones—comparison of recent theories with experimental-data, *Canadian Journal of Chemical Engineering* 71 (1993) 20–27.
- [20] R. Clift, M. Ghadiri, A.C. Hoffman, A critique of 2 models for cyclone performance, *AIChE Journal* 37 (1991) 285–289.
- [21] C.N. Davies, *Air Filtration*, Academic Press, New York, 1973.
- [22] M. Elimelech, J. Gregory, X. Jia, R.A. Williams, *Particle Deposition and Aggregation—Measurement, Modelling and Simulation*, Butterworth-Heinemann, 1995.
- [23] J. Lipowsky, M. Sommerfeld, Influence of particle agglomeration and agglomerate porosity on the simulation of gas cyclones, in: *6th International Conference on CFD in Oil & Gas, Metallurgical and Process Industries*, 2008.

- [24] M. Sommerfeld, S. Lain, From Elementary processes to the numerical prediction of industrial particle-laden flows, *Multiphase Science and Technologies* 21 (1–2) (2009) 123–140.
- [25] P.N. Brown, A.C. Hindmarsh, L.R. Petzold, Using krylov methods in the solution of large-scale differential-algebraic systems, *Journal Science Computers* 15 (1994) 1467–1488.
- [26] H.F. Meier, M. Mori, Gas–solid flow in cyclones: the Eulerian–Eulerian approach, *Computers Chemical Engineering* 22 (1998), sup 641–644.
- [27] R.B. Xiang, K.W. Lee, Numerical study of flow field in cyclones of different height, *Chemical Engineering Processing* 44 (2005) 877–883.
- [28] L. Svarovsky, J.C. Williams, T. Allen, in: *Handbook of Powder Technology*, Elsevier Scientific Publishing Company, New York, 1981.